Received: 19 April 2019 | Revised: 14 July 2021 | Accepted: 18 July 2021

DOI: 10.1002/esp.5209

RESEARCH ARTICLE

ESPL WILEY

How the capacity of bedrock to collect dust and produce soil affects phosphorus bioavailability in the northern Appalachian Mountains of Pennsylvania

Virginia Marcon[1] | Beth Hoagland[1,2] | Xin Gu[1] | Wenjing Liu[3,4] | Jason Kaye[5] | Roman A. DiBiase[1,6] | Susan L. Brantley[1,6]

[1]Department of Geosciences, The Pennsylvania State University, University Park, PA, USA

[2]Department of Geology and Geological Engineering, Colorado School of Mines, Golden, CO, USA

[3]Key Laboratory of Cenozoic Geology and Environment, Institute of Geology and Geophysics, Chinese Academy of Sciences, Beijing, China

[4]CAS Center for Excellence in Life and Paleoenvironment, Beijing, China

[5]Department of Ecosystem Science and Management, The Pennsylvania State University, University Park, PA, USA

[6]Earth and Environmental Systems Institute, The Pennsylvania State University, University Park, PA, USA

Correspondence
Susan L. Brantley, Department of Geosciences, The Pennsylvania State University, University Park, PA 16802, USA.
Email: sxb7@psu.edu

Funding information
Department of Geosciences, The Pennsylvania State: Hiroshi and Koya Ohmoto Fellowship 2017; U.S. National Science Foundation Division of Earth Sciences, Grant/Award Number: EAR 13-31726; Pennsylvania Department of Conservation and Natural Resources; National Science Foundation of China, Grant/Award Number: 41772380; Chinese Academy of Sciences, Grant/Award Number: XDB26000000; Pennsylvania State University; Youth Innovation Promotion Association CAS fellowship, Grant/Award Number: 2019067

Abstract

More above-ground biomass (kg m^{-2}) grows in the northern Appalachian Mountains (USA) in forests on shale than on sandstone at all landscape positions other than ridgetops. This has been tentatively attributed to physical (rather than chemical) attributes of the substrates, such as elevation, particle size, and water capacity. However, shales have generally similar phosphorus (P) concentrations to sandstones and, in the Valley and Ridge province, they erode more quickly. This led us to hypothesize that faster replenishment of the lithogenic nutrient P in shale soils through erosion + soil production could instead control the differences in biomass. To test this, soils and foliage from 10 sites on shales and sandstones in the northern Appalachians from roughly the same elevation and aspect were analysed. We discovered that, when controlling for location, concentrations of bioavailable P in soils and P in foliage were higher and P resorbed from senescing red oak leaves was lower on slower-eroding sandstone than on faster-eroding shale. Lower resorption generally can be attributed to lower P limitation for trees. Further investigation of weathering and erosion on one of the sandstone–shale pairs within a larger, paired watershed study revealed that the differences in P concentrations in biomass and foliage between lithologies likely developed because sandstones act as 'collectors' that trap nutrients from residual and exogenous sources, while shales erode quickly and thus promote production of soil from bedrock that releases P to ecosystems. We concluded that the combined effects of differential rates of dust collection and erosion results in roughly equal biomass growing on sandstone and shale ridgetops. This work emphasizes the balance between a landscape's capacity to collect dust versus produce soil in controlling bioavailability of nutrients.

KEYWORDS
biomass, chemical weathering, dust, erosion, foliage, nutrients, Shale Hills

1 | INTRODUCTION

The thin layer of Earth's skin extending from groundwater to tree canopy, known as the critical zone (CZ) (National Research Council, 2001), is deemed 'critical' at least partly because it provides nutrients necessary to support terrestrial life. Fully understanding the development, dynamics, and evolution of the CZ and its relationship to the environment and underlying substrates is crucial to sustaining human systems (e.g. Keestra et al., 2016). For example, lithogenic (rock-derived) nutrients such as phosphorus (P) can increasingly limit landscapes that are exposed for geologically long time periods (Chadwick et al., 1999; Hahm et al., 2014; Porder et al., 2007; Wardle et al., 2004). This occurs partly because P is occluded into recalcitrant material that remains in soils for long durations (e.g. Walker & Syers, 1976). Occlusion occurs as more readily available forms of P (e.g. Ca-bound P in primary minerals such as apatite) are depleted, and

P becomes incorporated into organic materials and on Fe- and Al-(oxy)hydroxides. Over time, inputs of P as apatite or other primary minerals from underlying rock also become lower than outputs in slowly eroding landscapes, creating a P-deficient soil (e.g. Porder et al., 2007). Thus, a paradigm has emerged that P availability in soils is lower in slowly eroding systems where soil residence times are long because the rate of supply of rock-derived P is slow, allowing the soil to lose P faster than it is replenished (for a review, see Arvin et al., 2017). The shift to more P-limited systems in soils with longer residence times over thousand- to million-year timescales is hypothesized to cause a decline in ecosystem productivity (Porder & Hilley, 2011; Porder et al., 2007; Wardle et al., 2004).

The Valley and Ridge physiographic province of the mid-Atlantic USA provides a natural laboratory to study inter-relationships among erosion rate, lithogenic nutrient abundance, and biomass. Researchers have observed that forests on shale grow faster and store more above-ground carbon than forests on sandstone in the northern Valley and Ridge (Reed & Kaye, 2020; Smith et al., 2017). An associated study on paired catchments on shale and sandstone located within the Susquehanna Shale Hills Critical Zone Observatory (CZO) similarly observed 60% more above-ground biomass on shale than sandstone in the same region (Brantley et al., 2018; Brubaker et al., 2018; Li et al., 2018). The difference in biomass between shale and sandstone (Brubaker et al., 2018; Smith et al., 2017) was exhibited in toe-slope, swale, and valley landscape positions, whereas above-ground biomass values on the ridgetops of the paired watersheds were similar (Table 1). Although noting that shales in the area might also have lower P concentrations than sandstones, Reed and Kaye (2020) proposed that the differences between biomass on shale and sandstone were largely attributable to physical attributes related to the substrates, such as topography, clay content, and water-holding capacity.

In this paper we investigate the alternate hypothesis that differences in P content or P flux through the soils on shales and

TABLE 1 Summary of effects of lithology and aspect

Lithology	Shale *Producer*	Sandstone *Collector*
Paired watershed sites	**Shale Hills**	**Garner Run**
Periglacial features	Subsurface fractures	Many above- and below-ground features
Erosion rate	~20 m Ma^{-1}	~7 m Ma^{-1}
Residence time of soil	~20 ka	~150 ka
Approximate percentage clay + silt in soil[a]	~40%	~20%
Bulk P in soils (Table S1)	0.15 ± 0.07 wt.% as P_2O_5	0.18 ± 0.19 wt.% as P_2O_5
Bedrock P (Table S1)	0.09 wt.% as P_2O_5	0.10 wt.% as P_2O_5
Total cation exchange capacity[b]	40 ± 4 meq/kg	23 ± 6 meq/kg
Average above-ground biomass[c]	22.4 ± 7 kg m^{-2}	14.1 ± 4 kg m^{-2}
Above-ground biomass at ridgetop[d]	15.8 ± 5.1 kg m^{-2}	14.5 ± 2.2 kg m^{-2}
The 10 study sites	**5 shale soils**	**5 sandstone soils**
Bioavailable P[e]	41 ± 8 mg/kg	60 ± 8 mg/kg
Live leaf P	0.12 ± 0.02%	0.15 ± 0.03%
Aspect	**Leading Ridge**	**Tussey Mountain mid-slope**
	North-facing (LRRT)	*South-facing (TMMS)*
Periglacial features	Some boulder fields	Many boulder fields and solifluction lobes
Pedogenic layers	Clay content peaks at 30–40 cm b.l.s.	No clay layers developed
Approximate percentage clay + silt in soil[a]	50%	25%
D_{50} (50% of particle diameters are smaller)	D_{50} = 53.8 μm	D_{50} = 237 μm
Bioavailable P[e]	63 ± 37 mg/kg	22 ± 19 mg/kg
Above-ground biomass[f]	14.5 ± 2.2 kg m^{-2}	11.0 ± 4 kg m^{-2}
Calc. contribution from Tuscarora[g]	~70%	~90%
Calc. contribution from dust/Castanea[g]	~20%	~10%
Calc. contribution from Rose Hill shale[g]	~10%	<1%

[a]Particles between 8 and 53 μm.
[b]Determined using $BaCl_2$ extract following the procedure outlined by Jin et al. (2010).
[c]Average watershed values summarized by Brubaker et al. (2018) for Shale Hills and Garner Run.
[d]Above-ground biomass at ridgetops as reported by Brubaker et al. (2018).
[e]Determined using Mehlich-III in the O-horizon of soil.
[f]Above-ground biomass at LRRT or TMMS as reported by Brubaker et al. (2018).
[g]Calculated as described in text and Marcon (2019).

sandstones in the region could instead explain the biomass observations. Specifically, erosion rates are generally higher for shales than sandstones, and this is especially true in the plunging folds of Paleozoic strata that define the northern Valley and Ridge, where shales (and limestones) define valleys and sandstones define ridges (Del Vecchio et al., 2018; Folk, 1960; Miller et al., 2013; Portenga et al., 2013). Specifically, with an erosion rate of E (mass m^{-2} $year^{-1}$) and P concentration in bedrock of C_P (mass $mass^{-1}$), the flux of P (mass m^{-2} $year^{-1}$) through the soil considered in a 1D model over timeframes much larger than the lifetimes of the resident vegetation equals C_PE. Given that shales have higher erosion rates than sandstones in the Valley and Ridge and often have similar or higher P concentrations than sandstones (Porder & Ramachandran, 2013), the rate of rejuvenation of P for the soil, C_PE, should be higher on shales than sandstones, and could provide an alternate explanation for the biomass observations in Table 1.

To explore this, we sampled soils within the same pair of neighbouring watersheds on shale and sandstone studied by Brubaker et al. (2018) within the CZO (Brantley et al., 2018) and nine additional shale and sandstone sites in the nearby northern Appalachians (all located in central Pennsylvania, USA). All 10 soils were analysed for nutrients, and the pair within the CZO were investigated more thoroughly within the context of ongoing research. Deeper understanding of the development of regolith in the two lithologically distinct and largely undisturbed headwater catchments in the Valley and Ridge within the CZO allowed us to quantify contributions to the soil in the catchment underlain by sandstone where soil residence times ≈ 150 ka (Del Vecchio et al., 2018) and the catchment underlain by shale where residence times ≈ 20 ka (Ma et al., 2010, 2013). We expand on earlier papers (Brantley et al., 2016; Hoagland et al., 2017) to elucidate weathering of the sandstone in comparison to previously published data for the shale catchment (Jin et al., 2010). Our geochemical and geological observations lead us to emphasize the importance of erosion-resistant lithologies such as sandstones that act as collectors of dust and residua, and how this affects their associated ecosystems.

2 | METHODS

2.1 | Ten distributed study sites

We sampled five sandstone and five shale sites in the Valley and Ridge region of Pennsylvania, including one shale and one sandstone site each in the Susquehanna Shale Hills CZO. All sites, sampled at the mid-slope position on north-facing aspects, were underlain by either Silurian Tuscarora sandstone (Hazleton or Hazleton association soil series) or Silurian Rose Hill shale (Berks or Berks association soil series). Site locations are summarized in Figure 1 (for further information see Table S2 and Hill (2017)).

2.2 | Critical zone observatory sites

We further investigated two of the sites that are part of monolithologic headwater catchments in the Susquehanna Shale Hills CZO (Figure 1). These two east–west trending catchments are located <5 km apart within the Shaver's Creek watershed of the Susquehanna River Basin (Brantley et al., 2018; Li et al., 2018).

The shale catchment, Shale Hills (SH, area ~0.08 km^2), is underlain by the ~200 m-thick Rose Hill Formation, a slightly metamorphosed greyish-buff shale that grades from shale to siltstone with some interbedded carbonate- and sand-rich strata (Folk, 1960). Shale Hills is the location of an ephemeral stream that empties into Shaver's Creek as part of the Susquehanna River basin.

Erosion rates were previously measured using meteoric ^{10}Be at 15–20 m Ma^{-1} (Jin et al., 2010; West et al., 2014) and a rough average of soil residence times from U disequilibrium isotope measurements is ~20 ka (Ma et al., 2010, 2013). Generally, soils in SH are deeper in the valley and along swales (1.5–3.0 m) and shallower along the ridges (0.2–0.3 m). The soil is derived from *in-situ* weathering of the underlying shale bedrock, with some development on colluvium towards toe-slopes. Soil is defined here as the regolith material that can be sampled by hand-augering and that lies above fractured

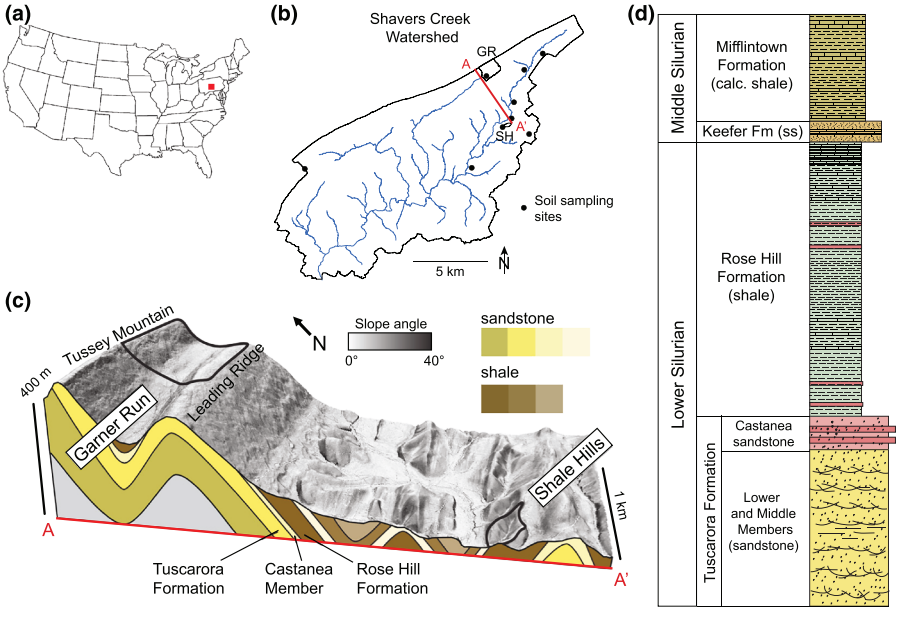

FIGURE 1 Site location of the two monolithologic headwater catchments and the additional shale and sandstone sites. (a) The two focus watersheds—Garner Run (GR), underlain by the Tuscarora sandstone, and Shale Hills (SH), underlain by the Rose Hill shale—are located in Central Pennsylvania, USA (red symbol). (b) GR and SH are located within the Shaver's Creek watershed, as are the four additional sandstone and four additional shale sites shown by black symbols. (c) Geological cross-section and block diagram showing the GR and SH watersheds (outlined in black). (d) Silurian-aged strata for the area. Location of the cross-section A–A′ in (c) is shown in red in (b). Geological cross-section is reproduced from Del Vecchio et al. (2018) [Color figure can be viewed at wileyonlinelibrary.com]

weathered rock (also referred to as saprock) and colluvium (Jin et al., 2010). Only mobile soil (no saprolite) has been observed within SH.

The second catchment, Garner Run (GR, area ~1.34 km^2), is completely underlain by the Tuscarora Formation, a slightly metamorphosed sandstone classified as orthoquartzite with minor interbedded clays (>95% quartz) (Cotter, 1983). The Tuscarora Formation has two members, the iron-rich Castanea sandstone and the lower and middle members that we refer to as the Tuscarora sandstone (Figure 1) (Folk, 1960). The Tuscarora Formation forms linear, erosion-resistant ridges throughout the Valley and Ridge and has a maximum thickness of 450 m (Cotter, 1983). GR is nestled within a synclinal structure where near dip-slopes define the hillslopes (Figure 1) and a first-order perennial stream (Garner Run) runs through the catchment. Erosion rates in the catchment have been estimated using *in-situ* ^{10}Be in stream sands at 6.6 m Ma^{-1} (Del Vecchio et al., 2018) (Table 1). This erosion rate was used to estimate soil residence times (1 m/6.6 m/Myr = 150 kyr). Gibbsite, an aluminium oxide that forms from aluminosilicates after solubilization of silica content, is observed within some GR soils, but missing from SH. This observation is consistent with older, more weathered soils present in GR (Hoagland et al., 2017). The soil in GR was defined as regolith above fractured but intact bedrock and no saprolite was observed. Soil was sampled in pits dug with shovels and a jack hammer to remove boulders (Brantley et al., 2016), but the estimates of soil thickness are minimum values. Despite the insoluble nature of the quartz-rich sandstone underlying the GR catchment, metre-thick soils have developed with significant concentrations of some elements (e.g. Al, Fe, K, Mg) (Figure 2) and clay relative to bedrock (Brantley et al., 2016; Hoagland et al., 2017).

The GR landscape exhibits many periglacial features such as boulder fields, solifluction lobes, relic landslides, and thick colluvial toeslope deposits (Brantley et al., 2016; Del Vecchio et al., 2018; Figure 3). Throughout the Pleistocene, repeated episodes of solifluction and mass wasting have led to net accumulation of colluvial valley fill deposits over timescales of >300 kyr (Del Vecchio et al., 2018). It is also likely that periglacial conditions throughout the Pleistocene promoted enhanced rates of subsurface fracturing via frost-cracking (Gardner et al., 1991), which could allow meltwater to move through the subsurface in periglacial climates (Tye et al., 2011). In comparison to GR, the topography of SH shows little evidence of surficial features

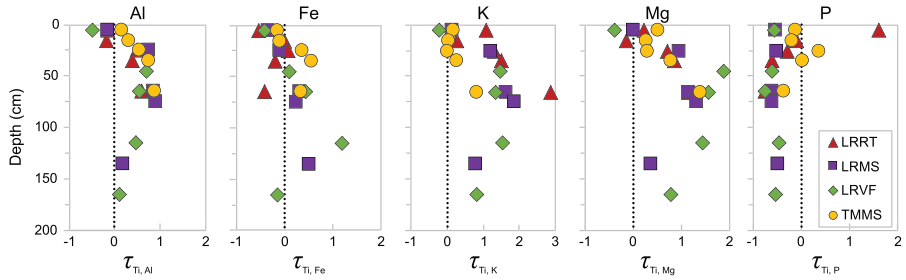

FIGURE 2 Normalized chemistry for soil profiles along the Garner Run catena. Bulk soil is generally enriched in Al, Fe, K, and Mg as compared to underlying bedrock ($\tau > 0$). Parent bedrock chemistry, used to define $\tau = 0$, is defined here from averages of deepest recovered rocks in each soil profile and borehole HV1 from the 4.9 to 6.4 m depth interval (data from Table S1; Brantley et al., 2016; Hoagland et al., 2017). Exact definition of parent composition is impossible because it has weathered/eroded away, but the soil contains more clay, Al, Fe, K, and Mg than the Tuscarora orthoquartzite. Lack of correct identification of parent is evident in that the τ values do not return to 0 (parent composition) at depth. This is especially true for low-concentration elements Mg and P [Color figure can be viewed at wileyonlinelibrary.com]

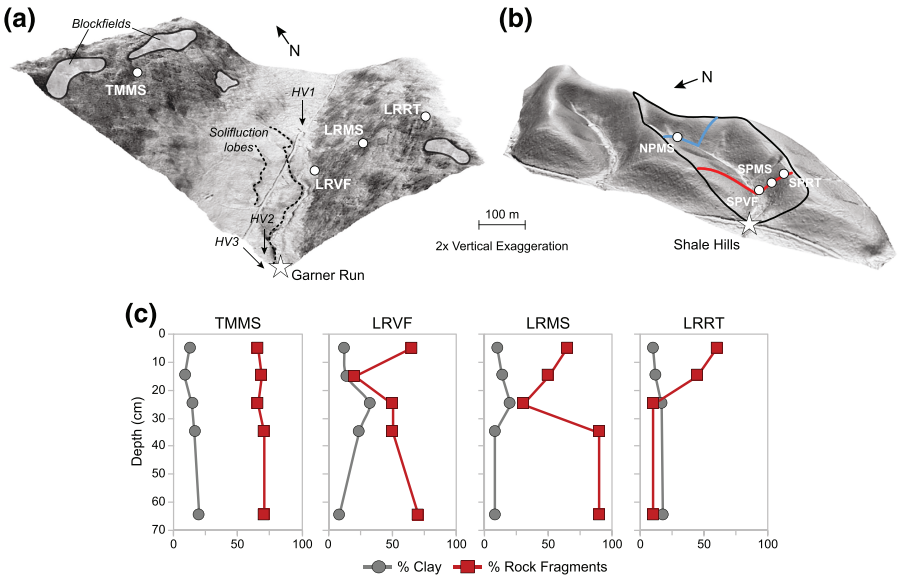

FIGURE 3 GR and SH catchments and field-determined particle sizes for GR. (a) GR watershed with the four soil pits shown in white circles, well locations shown with arrows, and the watershed outlet with a star. Block fields and solifluction lobes are outlined in solid black and dotted black lines, respectively. (b) SH watershed 2× vertical exaggeration (outlined in black) and soil sites in white circles; outlet denoted by a white star. (c) Relative clay and rock content plotted versus depth for the four soils in GR. In general, soils from the south-facing slope are more homogenized than those along the north-facing slope [Color figure can be viewed at wileyonlinelibrary.com]

resulting from periglacial climates: apparently, the rates of soil creep since the Last Glacial Maximum (LGM) at SH are large enough to largely obscure periglacial effects (West et al., 2014). In contrast, the catchment retains ample evidence of shallow subsurface fracturing and water flow (Brantley et al., 2013; Jin et al., 2010; West et al., 2019). Much smaller volumetric accumulations of sandy/silty sediments have been documented in the valley of SH and those sediments are younger than those in GR (Ma et al., 2010; West et al., 2014).

Periglacial processes also impose differences in soil transport and erosion with respect to aspect. Erosional efficiency and soil thickness can vary with aspect because of the higher solar radiation and more frequent freeze–thaw cycling on the sun-facing slope, especially during glacial periods (West et al., 2019). Thus, block fields and solifluction lobes are observed in GR to be less prevalent along north-facing than south-facing hillsides (Brantley et al., 2016). This aspect-related asymmetry is inferred to have resulted in faster net physical loss of material down the south-facing slope compared to the north-facing slope at GR, as evidenced by relic mass-wasting features. A somewhat similar pattern is observed at SH, where meteoric ^{10}Be and topographic data indicate that the erosional efficiency of the south-facing side is higher than the north-facing side of the watershed (although without block fields or identifiable solifluction lobes) (West et al., 2014).

Ridgetops on both catchments, characterized by mixed deciduous forests regenerated after widespread harvesting at the beginning of the 20th century, have similar biomass (Table 1). The trees are ~90–100 years old in GR and ~150 years old in SH. The overall SH watershed supports an oak–mixed hardwood forest dominated by *Quercus rubra* L., *Quercus prinus* L. syn, *Quercus montana*, *Quercus alba* L., Carya spp., and *Acer saccharum* marsh with sparse understory (Brubaker et al., 2018). GR supports a less diverse overstory dominated by *Q. prinus*, *Acer rubrum* L., *Betula lenta*, and more abundant understory. The understory in GR is made up of both deciduous and evergreen shrubs that are members of the Ericaceous family (Brubaker et al., 2018; Li et al., 2018). The greatest biomass is stored in Quercus spp. in both catchments (Brubaker et al., 2018), and the vegetation communities are similar to forests throughout the region (i.e. Brush et al., 1980).

2.3 | Chemical characterization of soils and rocks

Data from soils, bedrock, and borehole cores were either used as previously reported or were newly measured for each watershed (Figure 2). In both watersheds, soils were excavated (pits) or cored (auger holes) along roughly north–south transects across sub-planar hillslopes (Brantley et al., 2016). Most results for SH relate to the south planar and north planar hillslope catenas that are referred to with SP or NP as prefix for the naming convention (Brantley et al., 2018; Jin et al., 2010). The naming convention for both watersheds also refers to sites as ridgetop (-RT), mid-slope (-MS), or valley floor (-VF) (Figure 3). Thus, for SH, we refer to the north planar (NP) mid-slope site (NPMS) or south planar sites (SPRT, SPMS, SPVF). In GR, the north and south slopes are known locally as Tussey Mountain and Leading Ridge, respectively, and catena positions are thus referred to as TMMS (Tussey Mountain mid slope) or LRRT, LRMS, and LRVF (Leading Ridge ridgetop, mid-slope, and valley floor, respectively).

To understand bedrock lithology in GR, cored solids from three boreholes (HV1, HV2, and HV3) in the valley were also analysed. HV1, near the headwaters of Garner Run as shown in Figure 3, was drilled to 9 m b.l.s. (metres below land surface) through packages of unconsolidated sand and Tuscarora sandstone boulders (Del Vecchio et al., 2018; Hoagland et al., 2017). HV2 and HV3, located near the outlet of the GR subcatchment (Figure 3), were drilled to 4 and 2 m depth, respectively (Li et al., 2018). To compare to iron-rich sediments found within GR, we also collected samples in local outcrops of the Castanea Member of the Tuscarora Formation as a possible source of soils.

Soils and rocks were air-dried and then homogenized before further treatment. Bulk chemistry (Li metaborate fusion followed by analysis using a Perkin-Elmer Optima 5300 inductively coupled plasma atomic emission spectrometer), total carbon, nitrogen, hydrogen, and sulphur (Leco EA 1110 CHNS-O elemental analyser or CE Instruments EA 110 elemental analyser) were determined for some soils and cores. Where samples are noted as 'bulk' they included all recovered materials (even fragments >2 mm) that were then ground to particle sizes <150 μm for analysis.

Selected soil, parent, and sediment samples were also analysed by scanning electron microscopy (SEM; FEI Quanta 200 Environmental) using back-scattered electrons to evaluate mineralogy and grain shape and size (for details see Marcon, 2019).

2.3.1 | Bulk elemental depletion and enrichment

The extent of chemical weathering is often evaluated by calculating a mass transfer coefficient, $\tau_{i,j}$ [Equation 1] (Anderson et al., 2002; Brimhall & Dietrich, 1987). The mass loss or gain from an observed soil profile is determined by comparing the relative ratio of the concentration of an immobile element or mineral (*i*) to a mobile element or mineral (*j*) in the original unweathered parent rock (*p*) and overlying weathered material (*w*):

$$\tau_{i,j} = \frac{C_{i,p} \times C_{j,w}}{C_{j,p} \times C_{i,w}} - 1 \quad (1)$$

Interpretation of $\tau_{i,j}$ is based on the assumption of a parent chemistry and an immobile element (Anderson et al., 2002), which here was chosen as titanium. Parent chemistry is generally analysed on bulk samples that include rock fragments, as reported here.

2.3.2 | Bioavailable nutrients

To investigate Al- and Fe-phosphates and dissolved and adsorbed forms of P (Wolf & Beegle, 2011), nutrient bioavailability was determined using a Mehlich-III extract on soil samples sieved to <2 mm (Hill, 2017). For bioavailable N we measured ammonium plus nitrate extracted by 2 M KCl. These measurements were completed on samples from the O-horizon, 0–20 cm depth, and 20–40 cm depth of the north-facing mid-slope from the 10 soil sites underlain by the Tuscarora sandstone and Rose Hill shale, including GR and SH

(Figure 1). An additional set of analyses was completed on samples from TMMS (south-facing mid-slope) for comparison to north-facing LRRT (chosen because it has similar elevation to TMMS) to assess the importance of aspect to nutrient bioavailability in soils in GR.

Finally, to determine how soil chemistry affects foliage chemistry, ~200 live and senesced leaves were collected for two growing seasons (2015 and 2016) from red maples (*A. rubrum*) and red oaks (*Q. rubra*) near each of the five locations on sandstone and five locations on shale (Hill, 2017). Live leaves were collected by Winchester 1300 Pump Action shotgun and dead leaves were collected from litter traps (1 × 0.5 × 1.5 ft). Leaves were oven dried at 60°C for at least 48 h, ground, digested in nitric acid, and analysed by inductively coupled plasma atomic emission spectroscopy at the Penn State Agricultural Analytical Services Lab.

Nutrient resorption, the percentage of the leaf nutrient pool resorbed [Equation 2] (Boerner, 1984) was calculated from concentrations in live and senesced leaves:

$$\frac{[\text{Live leaves}] - [\text{Senesced leaves}]}{[\text{Live leaves}]} \times 100 \quad (2)$$

Red oak and red maple were analysed because they are ubiquitous throughout the northeast, and are found on both shale and sandstone lithologies in our study area.

2.3.3 | Mineralogy

Mineralogy of the parent, bulk soil, and clay separate fractions was evaluated using a PANanalytical Empyrean model powder by X-ray diffractometer (XRD) at the Penn State Material Science Laboratory X-Ray Crystallography facility. Changes in clay mineralogy in the bulk soil were estimated using the Shultz ratio (ratio of peak area at 19.9 and 26.6° 2θ) (Schultz, 1964).

2.3.4 | Particle size distribution and porosity

To determine particle size distributions as a function of aspect in soils of GR, subsamples of homogenized soils from south-facing (TMMS) and north-facing soils from similar elevations (LRRT) at depths of 10–20 cm, 30–40 cm, and 60–70 cm were sieved to <2 mm for particle size analysis using both automated imaging and dry dispersion laser diffraction methods (Table 3). Rock chips, epoxy grain mounts, and dispersed soil particles were also evaluated for particle size and shape by image analysis on SEM photomicrographs to provide information on particles ranging from 10 nm to 1 mm (Marcon, 2019).

Rock fragments recovered from multiple depths in the LRRT and LRVF pits were analysed for porosity (Figure 4) by neutron scattering and image analysis (Marcon, 2019). Combined small-angle and ultra-small-angle neutron scattering experiments were performed at the U.S. National Institute of Standards and Technologies. Neutron scattering provides information on the distribution of pores ranging in size from ~1 nm to 20 μm in diameter.

2.4 | Strontium isotopes

Strontium (Sr) isotopes were analysed as a conservative provenance tracer (Capo et al., 1998) on bulk soil samples from specific depth intervals from two GR soils [LRRT (10–20 cm, 30–40 cm, and 60–70 cm) and TMMS (10–20 cm, 30–40 cm, and 60–70 cm)]. Sr isotopes were also analysed on Rose Hill shale and Tuscarora sandstone, on weathered Tuscarora rock (recovered from LRRT at 45 cm depth), and on two samples from the Castanea member recovered in local outcrops outside of the CZO (Marcon, 2019). The latter was analysed as a possible parent for some iron-rich soil samples in the GR catchment. We also analysed particles recovered from the stream and groundwater in SH as described previously (Kim et al., 2018). These particles are interpreted to be weathered particles of Rose Hill Formation,

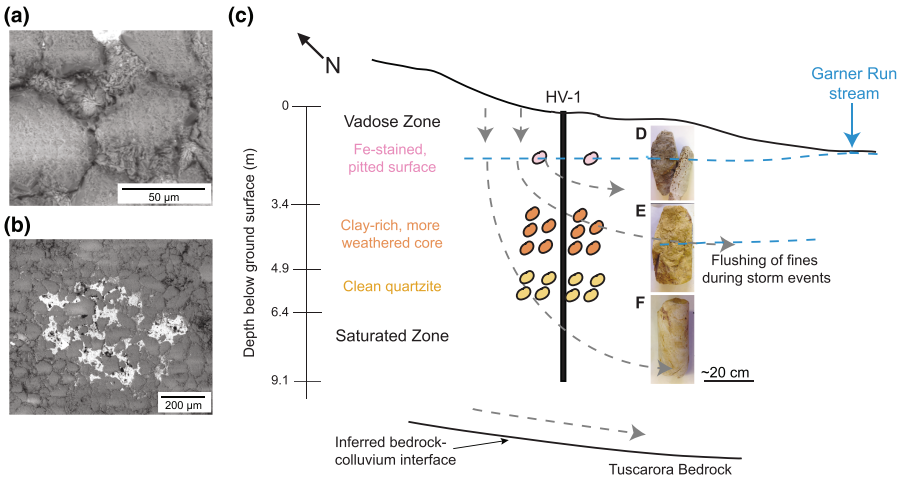

FIGURE 4 Schematic figure summarizing subsurface movement of clay and iron oxides in the Garner Run catchment. Scanning electron micrographs of sand grains in sandstone clasts recovered from deep within hillside soils show that clays (a) and iron-oxide particles (b) are trapped in the pores during weathering. (c) Subsurface transport of fine particles was also observed in groundwater sampled in borehole HV1 (see Figure 3 for location). Material recovered during drilling of the borehole was mostly unconsolidated sand with occasional sandstone clasts: clasts were iron-stained and pitted nearer the surface, clay-rich and highly weathered at mid-depths, and cleaner at depth (see Marcon (2019) for details). Figure not to scale [Color figure can be viewed at wileyonlinelibrary.com]

mobilized from the soil and from the weathered rock in the subsurface during storms, transported through the subsurface, and captured using high-interval automated sampling throughout the rising and falling limb of stream events. They were analysed as a proxy for particles that could have been derived from the previously eroded Rose Hill shale overlying the Tuscarora sandstone in GR (see Figure 1 for stratigraphy).

Bulk rock, particles, and soil samples were digested as per published procedures (Crock et al., 1983). An aliquot of the digested sample was analysed by Thermo Scientific iCAP RQ inductively coupled plasma mass spectrometry (ICP-MS) for total Sr and Ca in the Laboratory for Isotopes and Metals in the Environment (LIME) at Penn State University (uncertainties typically better than ±10% [2σ]). Strontium was purified from a second aliquot by an ESI Prepfast MC system and a proprietary ESI Ca-Sr resin (Romaniello et al., 2015). The $^{87}Sr/^{86}Sr$ ratios were determined using a Thermo Scientific Triton Plus thermal ionization mass spectrometer (TIMS), also housed in LIME. Instrumental mass bias on the $^{87}Sr/^{86}Sr$ ratios was corrected by using an exponential law applied to measurements of the $^{86}Sr/^{88}Sr$ ratio, with an assumed true ratio of 0.1194. For the period of analysis, reference NIST987 prepared with the PrepFast reported 0.710254 ± 0.000010 (1 std error), $n = 7$.

2.5 | Water chemistry

Ground and stream waters were sampled for different periods of time in both GR and SH. Some of these data have been discussed previously (Hoagland et al., 2017; Sullivan et al., 2016). Marcon (2019) presents a full description of wells and sampling procedures and the full dataset is available in the CZO online data portal (www.czo.psu.edu).

3 | RESULTS

3.1 | Soils and valley deposits versus parent rock

Defining parent material is the most challenging component of calculating the mass transfer coefficient, $\tau_{i,j}$, due to natural heterogeneities and stratigraphic variations and the limitation that the original parent material has weathered away. The parent chemistry for SH was based on averaging samples from four deep cores (Sullivan et al., 2016). The parent Tuscarora material for GR soil was calculated as the average of recovered rock from borehole HV1 and from new rock samples (Table S1) and previously published soil pit data (Brantley et al., 2016; Hoagland et al., 2017). However, this underlying 'parent' is not the only source of material to the soil, because the soils in GR are extremely enriched in most major elements relative to the Tuscarora Formation (i.e. $\tau > 0$; Brantley et al., 2016; Hoagland et al., 2017) (Figure 2). Inability to define parent composition accurately also explains why τ values do not generally return to parent ($\tau = 0$) at depth in the soils, especially for trace or minor elements. In contrast, most of these elements are depleted in the SH soils relative to the shale. As summarized in Tables 1 and S1, bulk soil P concentrations are similar between GR and SH.

As expected, the GR soils are sandy and dominated by quartz. But each profile is richer in clay (Figure 3) than the underlying bedrock, which generally has 1–5% clay content. Large clasts of the Tuscarora sandstone are also distributed throughout each profile (Figure 3c).

We observed some differences in mineralogy in the GR catena as a function of aspect. Generally, soil samples collected on the north-facing side have more clay minerals (illite, vermiculite) than soils on the south-facing side (Marcon, 2019). We also observed that the clay content varies (Schultz ratio varies with depth) in the north-facing soils (Table 3). In addition, XRD on bulk samples reveals the presence of albite, goethite, and K-feldspar in the north-facing soils (LRMS) (Marcon, 2019).

Boreholes drilled near the headwaters (HV1) and outlet (HV2, HV3) of Garner Run stream (Figure 3) intersect distinct packages of solid material (Del Vecchio et al., 2018; Hoagland et al., 2017; Marcon, 2019). In general, sediments recovered higher in the watershed from HV1 are sandy with few fines, while sediments recovered lower in the watershed from HV2 and HV3 are clay-rich with higher iron concentrations. However, a few rock clasts were recovered from HV1 at several depths. Rocks between 3 and 4 m depth were significantly darker in colour with higher Al, Fe, and Ti and lower Si concentrations (Figure 4c, Table S1) as compared to clasts above and below this interval (Del Vecchio et al., 2018; Marcon, 2019). These clasts are also more friable than elsewhere in the borehole.

3.2 | Soil nutrient availability and vegetation

Locations and data for the 10 shale and sandstone sites are summarized in Tables S2, S3 and in Hill (2017). To determine whether bioavailable soil nutrient concentrations differed across the 10 distributed locations, we used a nested analysis of variance (Proc GLM, SAS 9.4) with lithology type (shale vs. sandstone) and location (each of the 10 sampling sites was a location) nested within lithology type as the main effects. To test whether red maple and red oak foliar nutrient concentrations and resorption differed across the 10 distributed locations, we used a mixed model with location as a random effect and fixed effects of tree species, lithology type, and year.

Based on these statistical analyses, bioavailable Mg, Ca, S, and K concentrations were higher in the soils on shales than on sandstones (Table S2). Cu and Zn showed no significant difference between lithologies. In contrast, bioavailable P concentration was higher in soils on the sandstones (Figure 5, Table 2, $p < 0.05$). Table 2 also shows that in GR soils, nutrient bioavailability is higher on the north-facing than south-facing hillslope.

Live leaf chemistry also differs between the sandstone and shale sites (Table 2; all results collated in Table S3) (Hill, 2017). Concentrations of Ca, Mg, Zn, and Cu are all lower in live leaves recovered from the sandstone as compared to shale sites ($p < 0.05$). Only P is higher in the foliage from sandstone soils ($p < 0.05$). No significant difference was observed between lithologies for N content in live leaves.

The resorption of most nutrients [as defined in Equation 2] in leaves growing on sandstones is equal to or higher than resorption in leaves on shale, except for P in red oak (Table 2). Finally, the ratio of percentage resorbed N to percentage resorbed P in red oak trees is higher on sandstone relative to shale.

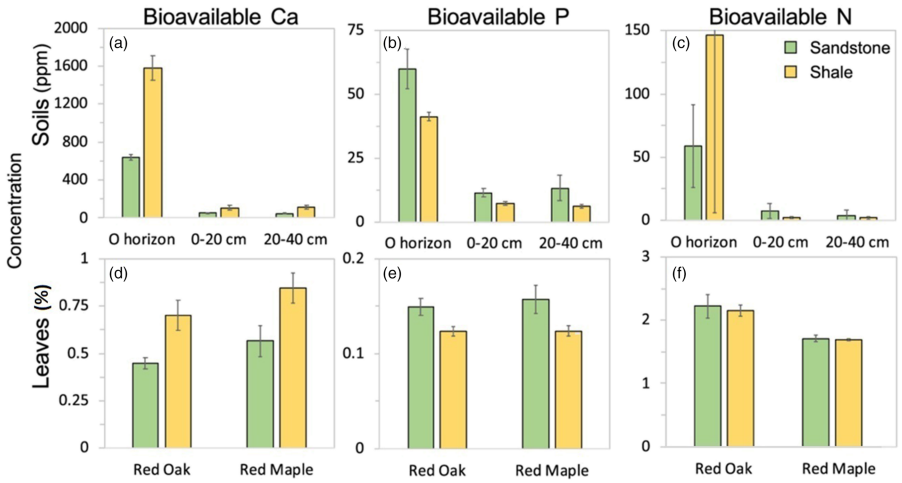

FIGURE 5 Concentrations of bioavailable calcium (Ca), phosphorus (P), and nitrogen (N) in soils (upper panels) and Ca, P, and N in live leaves (lower panels) from five sandstone (green) and five shale (yellow) sites. Generally, shale soils contain more bioavailable nutrients such as calcium and nitrogen; however, P, a lithogenic nutrient, is more bioavailable in sandstone soils than shale soils. P concentrations in live leaves collected from sandstone sites are also higher than in leaves collected from shale sites. Error bars are one standard error of the mean [Color figure can be viewed at wileyonlinelibrary.com]

3.3 | Particle size and porosity

Particle size distributions determined by several methods generally show that, as expected, soils from SH are finer than the sandy soils of GR (Table 3, Figure 3). At GR, soils from the north-facing hillslope (LRRT) are also generally finer-grained than soils from the south-facing hillslope (TMMS) (Table 3).

The relative fraction of porosity (size range: micron- to nanometre-sized) in nine rock fragments collected from different depths in GR soils range from 2.7 to 5.2% (Table 3). Although total porosity is low, 70–75% of the pores are water accessible (connected porosity), as determined by contrast-matched neutron porosity measurements (for a full discussion see Marcon, 2019). SEM photomicrographs of sandstone clasts recovered from various depths in HV1 and in the soil pits revealed ample evidence of weathering in the form of surface pitting. In addition, the outer rinds of clasts were often redder than the interior parts of the clasts. Under SEM it was observed that these rinds were characterized by pores that were filled with clays (Figure 4a) or iron oxides (Figure 4b).

3.4 | Strontium isotopes

Previously, three parent compositions (Tuscarora sandstone, dust, overlying Rose Hill shale) were hypothesized for GR soils (Brantley et al., 2016). Estimates of strontium (Sr) isotopic ratios of samples of these endmembers are compared with measurements for soil and for average dust in Figure 6. Dust values were estimated very roughly from ranges for North America (e.g., Aarons et al., 2017; Grousset & Biscaye, 2005; Marcon, 2019). Because we found a clast of a Castanea member of the Tuscarora Formation in the GR valley, we also collected and analysed samples of Castanea for Sr isotopes as another possible parent composition. We observed that three endmembers are distinguishable by their Sr concentrations and isotope ratios: (i) dust, (ii) particles from the overlying but eroded-away Rose Hill Formation, and (iii) the lower and middle members of the Tuscarora Formation (Figure 6a). The measured value for the iron-rich Castanea member of the Tuscarora Formation is not easily distinguished from the North American dust estimate and so, dust and Castanea are discussed as one possible source (Figure 6; Table 4).

Given these possible sources, TMMS soils cluster together between Rose Hill (0.7456 ± 0.0035) and Tuscarora (0.7204 ± 0.0054) at 0.7283 ± 0.0011 (ranging from 0.7296 to 0.7276). LRRT soils range from 0.7234 to 0.7352, between Rose Hill and Castanea (0.7135 ± 0.0023) + dust (0.7122 ± 0.0045) endmembers (Table 4). Weathered Tuscarora (LRRT 45 cm-depth rock) and Rose Hill (shale particles from SH groundwater) show similar $^{87}Sr/^{86}Sr$ ratios compared to underlying bedrock (LRRT = 0.7229 ± 0.0056; mobilized shale particles = 0.7344 ± 0.0016).

3.5 | Water chemistry

Iron concentrations (filtered through a 0.45 μm filter) in groundwater sampled in the upper part of the GR catchment (borehole HV1, Figures 3 and 7) at 9 m depth below land surface varied significantly (0.01–17 μg/mL) while turbidity was high (>1000 FTU) during the first 2 years after drilling (2015–2017). After 2017, the iron concentrations stabilized to an average of 0.18 ± 0.15 μg/mL (Table S4) and turbidity subsided to ≤10 FTU (Marcon, 2019). Water chemistry for these wells is reported and updated at http://www.czo.psu.edu.

However, some differences in turbidity of waters were observed over time as a function of depth in the three nested wells in HV1 (Figure 4). For example, pulses of high turbidity were observed after storm events in the 6 m well. Specifically, the turbidity increased in the 6 m well from 100 to 300 FTU following the storms related to Hurricane Florence in September 2018, while the turbidity remained below 5 FTU in the 9 m well. The depth interval sampled by the 6 m well corresponds with a sequence of corestones that were recovered during drilling that appear highly weathered compared to recovered corestones from above and below, as shown in Figure 4 (also see Del Vecchio et al., 2018).

4 | DISCUSSION

4.1 | Erosion and biomass

We hypothesized that the fast erosion rates of Valley and Ridge shales might explain why biomass is greater (mid-slope, toe-slope,

TABLE 2 Bioavailable soil nutrients measured as the total concentrations of C and inorganic N in soil (<2 mm fraction) and pH, acidity, P, K, Mg, Ca, Zn, Cu, and CEC measured using Mehlich-III extracts; as well as total nutrient concentrations in live and dead (senesced) tree leaves (mg kg^{-1} or percentage by mass of dry soil)

Pit	Depth (cm)	pH	Acidity index	Total N (ppm)	Total C (%)	P (ppm)	K (ppm)	Mg (ppm)	Ca (ppm)	Zn (ppm)	Cu (ppm)	S (ppm)	Bio CEC[†]
Bioavailable nutrients in Garner Run soils by aspect													
LRRT	O-horizon	4.7	11	54 ± 9.4	–	53	170	46	181	3.8	1.0	15.5	12.2
North-facing	0–20	4.1	15	8.9 ± 8.7	–	104	115	35	160	3.3	0.90	20.0	16.1
	20–40	4.5	6.9	2.9 ± 1.3	–	33	33	7.0	33.9	3.8	0.90	49.7	7.2
Average ± std		**4.39 ± 0.3**	**11 ± 3.9**	**22 ± 25**	–	**63 ± 37**	**106 ± 69**	**29 ± 20**	**125 ± 80**	**3.6 ± 0.3**	**0.93 ± 0.06**	**28.4 ± 18.6**	**11.8 ± 4.5**
TMMS	O-horizon	4.1	15	–	–	43	209	60	305	3.6	0.9	21.5	17.6
South-facing	0–20	4.0	12	–	–	12	28	13	42	2.2	1.3	26.0	12.7
	20–40	4.4	7.5	–	–	10	25	7	33.2	2.2	1.1	33.4	7.8
Average ± std		**4.13 ± 0.2**	**12 ± 3.9**	–	–	**22 ± 19**	**87 ± 105**	**27 ± 29**	**127 ± 155**	**2.7 ± 0.81**	**1.1 ± 0.20**	**27 ± 6.0**	**12.7 ± 4.9**
Bioavailable nutrients in soils averaged over five catchments[‡]													
Sandstone	O-horizon	4.2 ± 0.32	18 ± 4.4	65 ± 29	47 ± 1.1	60 ± 7.8	334 ± 34	99 ± 29	640 ± 140	10 ± 5.0	1.1 ± 0.09	29 ± 5.2	19 ± 1.2
	0–20	3.6 ± 0.23	15 ± 4.1	7.5 ± 5.9	2.8 ± 3.1	11 ± 4.6	59 ± 25	18 ± 5.0	52 ± 11	2.5 ± 1.2	0.90 ± 0.24	11 ± 4.2	14 ± 2.1
	20–40	3.8 ± 0.29	13 ± 4.5	3.8 ± 3.9	2.7 ± 1.7	13 ± 14	44 ± 20	16 ± 4.8	48 ± 14	2.3 ± 1.1	0.92 ± 0.38	12 ± 6.3	12 ± 3.0
Average ± std		**3.9 ± 0.38**	**16 ± 4.6**	**25 ± 33**	**20 ± 22**	**37 ± 40**	**160 ± 140**	**50 ± 44**	**290 ± 300**	**5.6 ± 5.1**	**0.99 ± 0.26**	**19 ± 10**	**16 ± 3.6**
Shale	O-horizon	5.2 ± 0.40	9.5 ± 2.8	150 ± 140	43 ± 2.5	41 ± 8.4	295 ± 61	210 ± 60	1600 ± 660	9.6 ± 3.3	1.0 ± 0.12	24 ± 4.6	20 ± 3.1
	0–20	4.5 ± 0.19	12 ± 2.1	2.0 ± 0.71	3.0 ± 1.6	7.2 ± 3.5	63 ± 17	34 ± 12	110 ± 84	2.7 ± 0.67	1.1 ± 0.34	16 ± 3.2	13 ± 1.89
	20–40	4.5 ± 0.29	12 ± 2.9	2.2 ± 1.2	2.6 ± 1.4	6.0 ± 2.4	60 ± 23	36 ± 15	120 ± 81	2.6 ± 0.96	1.0 ± 0.15	16 ± 3.3	12 ± 2.4
Average ± std		**4.7 ± 0.46**	**11 ± 2.8**	**50 ± 110**	**16 ± 19**	**18 ± 17**	**140 ± 120**	**94 ± 91**	**600 ± 290**	**5.0 ± 3.4**	**1.1 ± 0.23**	**19 ± 5.1**	**15 ± 4.2**
Nutrient concentrations in leaves from five sandstone and five shale catchments[‡§]													
Sandstone	Leaf type			N (%)	C (%)	P (%)	K (%)	Mg (%)	Ca (%)	Zn (ppm)	Cu (ppm)	S (%)	
	Live RO			2.2 ± 0.2	47 ± 1.4	0.15 ± 0.02	0.81 ± 0.15	0.11 ± 0.02	0.45 ± 0.09	22 ± 3.2	5.1 ± 0.75	0.14 ± 0.02	–
	Dead RO			0.72 ± 0.2	49 ± 3.7	0.11 ± 0.03	0.33 ± 0.09	0.09 ± 0.02	0.69 ± 0.09	25 ± 4.4	3.2 ± 0.54	0.07 ± 0.01	–
	Resorbed RO			*0.67 ± 0.1*	*−0.03 ± 0.1*	*0.24 ± 0.11*	*0.59 ± 0.12*	*0.21 ± 0.15*	*−0.58 ± 0.25*	*−0.12 ± 0.2*	*0.37 ± 0.09*	*0.48 ± 0.08*	–
	Live RM			1.7 ± 0.2	48 ± 1.5	0.16 ± 0.03	0.64 ± 0.15	0.13 ± 0.02	0.57 ± 0.18	18 ± 3.6	6.3 ± 1.3	0.11 ± 0.01	–
	Dead RM			0.70 ± 0.2	46 ± 4.5	0.07 ± 0.01	0.23 ± 0.08	0.11 ± 0.03	0.90 ± 0.28	23 ± 4.6	7.6 ± 1.8	0.06 ± 0.01	–
	Resorbed RM			*0.59 ± 0.1*	*0.02 ± 0.1*	*0.54 ± 0.13*	*0.64 ± 0.09*	*0.17 ± 0.15*	*−0.62 ± 0.27*	*−0.30 ± 0.2*	*−0.26 ± 0.40*	*0.42 ± 0.12*	–
Shale	Live RO			2.2 ± 0.2	47 ± 1.8	0.12 ± 0.02	0.83 ± 0.12	0.15 ± 0.04	0.70 ± 0.17	27 ± 6.5	5.8 ± 0.46	0.13 ± 0.01	–
	Dead RO			0.79 ± 0.1	48 ± 3.3	0.05 ± 0.01	0.34 ± 0.03	0.15 ± 0.04	0.96 ± 0.16	30 ± 7.6	3.5 ± 0.63	0.07 ± 0.01	–
	Resorbed RO			*0.62 ± 0.1*	*−0.03 ± 0.1*	*0.60 ± 0.08*	*0.59 ± 0.06*	*0.02 ± 0.20*	*−0.40 ± 0.17*	*−0.16 ± 0.3*	*0.39 ± 0.08*	*0.45 ± 0.09*	–

(Continues)

TABLE 2 (Continued)

Pit	Depth (cm)	pH	Acidity index	Total N (ppm)	Total C (%)	P (ppm)	K (ppm)	Mg (ppm)	Ca (ppm)	Zn (ppm)	Cu (ppm)	S (ppm)	Bio CEC[†]
	Live RM			1.7 ± 0.1	47 ± 1.7	0.12 ± 0.01	0.71 ± 0.17	0.18 ± 0.04	0.85 ± 0.17	29 ± 4.4	7.1 ± 1.9	0.11 ± 0.01	-
	Dead RM			0.90 ± 0.1	45 ± 4.8	0.06 ± 0.02	0.25 ± 0.05	0.17 ± 0.05	1.35 ± 0.16	40 ± 6.3	7.5 ± 2.4	0.09 ± 0.01	-
	Resorbed RM			0.47 ± 0.1	0.04 ± 0.1	0.52 ± 0.10	0.63 ± 0.10	0.01 ± 0.3	−0.64 ± 0.29	−0.38 ± 0.3	−0.11 ± 0.36	0.25 ± 0.09	-

RO = red oak.
RM = red maple.
Std = standard deviation.
[a]Determined using Mehlich-III extract (meq/100 g).
[b]Full dataset in Tables S2 and S3.
[c]Averaged over 2015 and 2016 seasons.

valley) or the same (ridgetops) on shales as compared to sandstones (Brubaker et al., 2018; Reed & Kaye, 2020). However, as compared to shales, P concentrations were measured to be larger in foliage grown on sandstones and bioavailable P concentrations were measured to be greater in soils on sandstones when locations were controlled for (Table 2, Figure 5). We also observed that red oak trees on sandstones resorbed a lower percentage of leaf P relative to N as compared to leaf resorption observed on shale soils (Table 2). This is consistent with the idea that red oak trees on sandstones are more N-limited than P-limited as compared to the trees on shale. In addition, when we studied soils and vegetation in watersheds on a slowly eroding sandstone (GR) and a faster-eroding shale (SH) within the Susquehanna Shale Hills CZO, we observed that the sandstone soils (residence time of ~150 ka) have roughly similar bulk P concentrations (Table 1) as the shale soils (residence time of ~20 ka), despite roughly similar P concentrations in the two parent rocks. We thus concluded that the faster erosion rates (and P rejuvenation rates) of shales alone cannot explain differences in biomass between shales and sandstones.

One reason why the older, slowly eroding lithology is not more depleted in bioavailable P could be because of atmospheric inputs. Worldwide, dust accumulation is known to influence soil texture, structure, and chemistry (Derry & Chadwick, 2007; Lawrence & Neff, 2009), weathering fluxes (Porder et al., 2007), terrestrial productivity (Kennedy et al., 1998), and microbial and plant community structure (Farmer, 1993). For example, dust sourced from Africa is thought to contribute a constant source of P in the Amazon forest, delaying P depletion for decades to centuries (Yu et al., 2015).

Previously, Ciolkosz et al. (1990) argued that ridges in the northern Appalachians act as natural dust traps and Brantley et al. (2016) suggested that soil in GR might be partly derived from dust. Specifically, the synclinal nature of the subsurface of GR and the rigid sandstone boulders on hillsides could have trapped exogenous inputs (Figures 1 and 7). Furthermore, recent models have shown that dust could have been an important source of nutrients for soils in the northeastern USA, especially during the LGM (Arvin et al., 2017). However, in non-tropical eroding systems, only a few studies have shown that dust is important as compared to the nutrients released to soil from bedrock weathering (e.g. Aciego et al., 2017).

In the following sections, we first explore the different possible sources to the GR soils, and then we explore the inter-relationships among erosion, soil formation, nutrient cycling, and subsurface particle transport in the GR and SH catchments to understand the biomass observations.

4.1.1 | Tuscarora formation as a source

Ample evidence can be cited that the Tuscarora is one of the parent materials that have contributed to the soils in GR: the high quartz content in the soils, pitting features on Tuscarora corestones (Marcon, 2019), similarity in morphology of some grains in soils and bedrock, and the presence of Tuscarora boulders within soils and at the surface are all direct evidence of chemical and physical weathering of the Tuscarora (Figure 6).

To explore this, we compare the Tuscarora (with a density of 2.65 g cm^{-3} and approximately 1–5% clay) with the average GR soil

TABLE 3 Average particle size (microns) and Schultz ratios

Pit	Depth (cm)	D_{50} LD	D_{50} AI	%Clay[a]	%Silt[a]	%Sand[a]	SEMc	Total porosity	Connected porosity	Schultz ratio
TMMS	10–20	263	182	6	14	82				ND
	30–40	126	140	12	25	63				ND
	60–70	312		4	13	83	44 ± 53			ND
LRRT	10–20	70.5	64.7	11	33	56		2.7%		0.017
	20–30							4.6%		
	30–40	36.5	83.8	19	29	51		2.8%		0.081
	40–60							5.2%	4.0%	
	60–70	54.4		33	28	49				0.213
LRMS	0–10									0.022
	60–70									0.064
	130–140	234					7.4 ± 14			0.025
LRVF	10–20							2.7%		
	20–30							2.7%		
	70–80							4.1%	2.9%	
	110–120							4.3%	3.2%	
	175							2.8%		
GR upper sediments							9.6 ± 12			
Shale Hills[b]				18	18	64				
Shale Hills[b]				23	14	63				

LD = particle size distribution by laser diffraction method.
AI = particle size distribution by automated imaging (AI-Morphologi G3SE).
ND = non detect.
[a]Calculated from dry dispersion (Malvern Mastersize 3000).
[b]Brantley et al. (2016).
[c]Average particle size determined from image analysis of SEM micrographs using Image J software.

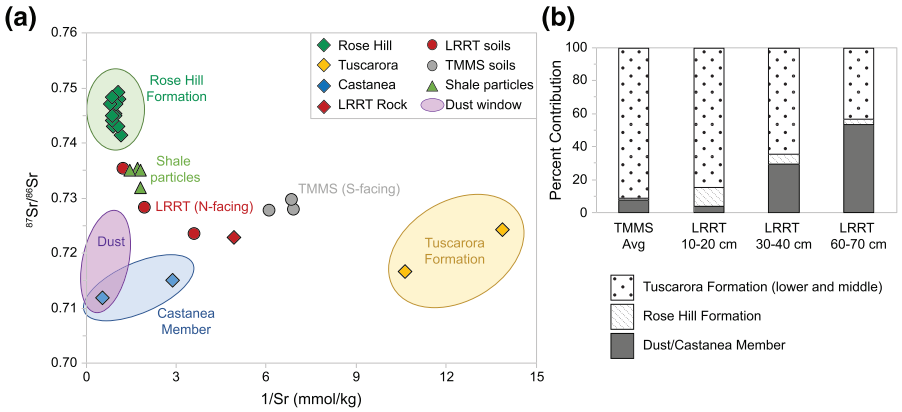

FIGURE 6 Strontium isotope signatures and potential sources of soils. (a) All GR soils (labelled LRRT, TMMS) are bounded by three putative parent endmembers: Rose Hill shale (green), Tuscarora sandstone (yellow, i.e. the lower and middle members of the Tuscarora formation), and a final endmember that we did not distinguish between the Castanea member of the Tuscarora formation and a generalized North American atmospheric dust (blue and purple, respectively). The ellipses are schematic zones roughly encircling source signatures. (b) Estimated contributions of Tuscarora, Rose Hill, and dust/Castanea in GR soils (average south-facing mid-slope soil TMMS, and for different depth intervals for north-facing ridgetop soil LRRT). Deeper LRRT soils contain more Tuscarora and less Castanea + dust + RH shale. Rough averages for TMMS and LRRT are reported in Table 1 [Color figure can be viewed at wileyonlinelibrary.com]

TABLE 4 Strontium isotope measurements

Site	Sample	IGSN	Mid-point depth (m)	Sr	$^{87}Sr/^{86}Sr$	1 SE
GR soil	LRRT 10–20	SSH0002JT	0.15	0.28	0.72348	3E-06
	LRRT 30–40	SSH0002JV	0.35	0.58	0.72824	4E-06
	LRRT 60–70	SSH0002JY	0.65	0.81	0.73524	4E-06
	TMMS 10–20	SSH0002L3	0.1	0.16	0.72755	6E-06
	TMMS 30–40	SSH0002L5	0.35	0.14	0.72781	4E-06
	TMMS 60–70	SSH0002L8	0.65	0.15	0.72960	1E-05
Castanea	HV3 110–113	SSH00037D	1.2	1.94	0.71190	5E-06
	Whipple Dam	SSH00036O	Outcrop	0.35	0.71514	6E-06
Tuscarora Parent	LRRT 60–70 rock	SSH0002JQ	0.65	0.20	0.72290	4E-06
	HV1 16–21A	SSH00038F	23.5	0.09	0.71659	6E-06
	GR streambed rock	SSH00036H	Outcrop	0.07	0.72430	5E-06
Rose Hill Shale Parent	DC3 42–43	SSH000SXB	13.0	1.12	0.74211	5E-06
	DC1 21[a]	SSH000SVZ	4.6	1.27	0.74537	–
	DC1 36[a]	SSH000SWE	21.4	1.27	0.74919	–
Mobilized Rose Hill shale particles	71		–	0.59	0.73546	1E-05
	73		–	0.55	0.73192	1E-05
	75		–	0.55	0.73502	1E-05
	79		–	0.69	0.73500	9E-06
Dust				0.91[b]	0.713[c]	
				5.92[b]	0.730[c]	

[a]Meek et al. (2016); average DC1 and DC3 unweathered $^{87}Sr/^{86}Sr = 0.74558$.
[b]Range, North America (Aarons et al., 2017).
[c]Range, North America (Grousset & Biscaye, 2005).

density of 1.5 g cm^{-3} and 14% clay (Figure 3; Table 3). Each metre of soil would require weathering at least 2–8 m of Tuscarora sandstone to accumulate the clays observed in the soil, and this would only be accomplished under the unlikely scenario that all the quartz was removed and all the clay remained. Using previously measured chemical weathering rates of 0.2–0.3 cm ka^{-1} for sandstones in the region (Alexander, 1985; Sevon, 1984), it would take 0.5–4 Ma to accumulate the observed clay and to remove the accompanying quartz. This time period is longer than the estimated residence times for hillslope soils based on cosmogenic isotopes in GR (150 ka) (Del Vecchio et al., 2018). Therefore, another source of clay is necessary to create the soils.

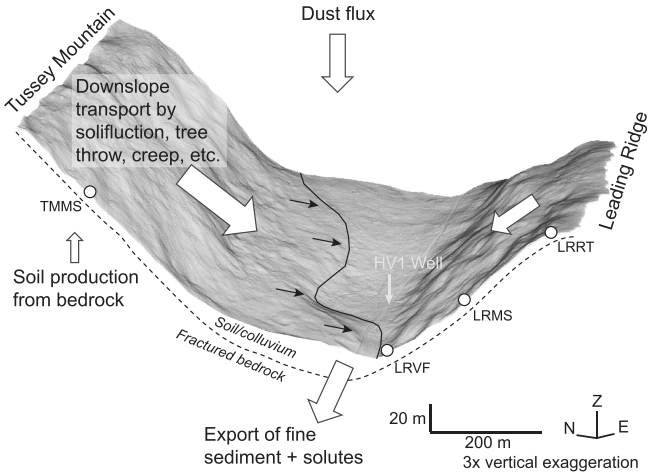

FIGURE 7 Perspective view of Garner Run subcatchment showing LiDAR bare-earth topography and interpretation of sediment mass balance. The south-facing Tussey Mountain hillslope is characterized by solifluction lobes that lead to more exposure of boulder fields than on the north-facing Leading Ridge hillslope (Del Vecchio et al., 2018). Soil pits are shown as open circles on the Tussey Mountain (TMMS) and Leading Ridge (LRVP, LRMS, LRRT) hillslopes. Downslope soil fluxes are interpreted to be higher on the Tussey Mountain side than the Leading Ridge side, but both hillslopes retain clay-rich soil interspersed with boulders and boulder fields. Fine particles and solutes are lost from the valley through the stream (Garner Run) and in groundwater, as inferred from observations at 6 m depth in well HV1 in Figure 4

4.1.2 | Evidence of exogenous inputs to GR soils

The most direct line of evidence for sources of material to the GR soil other than the Tuscarora Formation is the observation of meter-thick soils enriched in Al, Mg, Fe, and K (Figure 2) and clay (Figure 3, Table 3) as compared to the underlying bedrock. This observation is consistent with similar sites throughout the Valley and Ridge (Ciolkosz et al., 1990). Strontium isotopes are also consistent with the conclusion that GR soils likely did not form strictly from underlying bedrock (Figure 6).

In addition, the deeper LRRT soils also show evidence of clay bridging and a clay-rich B-horizon, features not expected to develop on soils on an orthoquartzite, but that might develop with exogenous inputs of clay. We hypothesize that the clays found at depth in the LRRT soil are illuviated clay particles derived from above. We observed some of this clay retained in pores in buried rocks in the soils (Figure 4). In addition, the Sr isotopic ratios in deep LRRT soils (maroon circles, Figure 6) approach the ratios measured in particles winnowed from Rose Hill shale in the SH catchment (green triangles, Figure 6). The soils on the north-facing side also show more contribution from exogenous materials than soils on the south-facing side based on Sr isotope data (Figure 6). This trend is likely preserved on the more stable north-facing slope as compared to the south-facing slope where relic mass-wasting events are evident.

4.1.3 | Accumulation of fines from overlying weathered material

One potential clay source for GR soils is residuum from the stratigraphically younger and previously eroded Rose Hill Formation. For example, soils from both sides of GR incorporate material more enriched in ^{87}Sr than Tuscarora and show $^{87}Sr/^{86}Sr$ ratios that are similar to mobilized particles recovered from SH stream water (i.e. Rose Hill Formation; Figure 6). Furthermore, the iron-rich particles and clays observed to clog pores in clasts of the Tuscarora sandstone recovered from soil pits and valley fill are broadly similar to particles mobilized out of the overlying iron-rich Rose Hill Formation (Bern & Yesavage, 2018; Kim et al., 2018; Yesavage et al., 2012). Similarly, clay bridging observed in ridgetop soils at GR (Brantley et al., 2016) could be evidence of clay illuviation from the overlying Rose Hill shale to form an argillic zone (Elliott & Drohan, 2009). The peak in clay-size particles in LRRT soils coincides with the highest $^{87}Sr/^{86}Sr$ isotopic ratios (i.e. ratios similar to the Rose Hill Formation; Figures 3 and 6; Table 3). $^{87}Sr/^{86}Sr$ ratios within LRRT soils also trend towards Rose Hill bedrock with depth, again consistent with retention of shale particles (albeit with illuviation within the pedon) in soils along that ridgetop. Pedogenic layers and argillic zones are not common in soils that are strictly quartzite-derived (Elliott & Drohan, 2009).

In contrast to soils on the north-facing slope, the soil from the south-facing slope (TMMS) shows $^{87}Sr/^{86}Sr$ ratios that are more like the Tuscarora sandstone and less like the Rose Hill Formation (Figure 6). These soils also appear well mixed because they have similar $^{87}Sr/^{86}Sr$ ratios at all depths. These characteristics are consistent with the greater occurrence of mass-wasting events along Tussey Mountain that may have removed overlying more developed soils or homogenized extant soils (Figures 3 and 7).

Pedogenic layers, clay bridging, and strontium isotopic signatures in LRRT soils indicate a stable north-facing hillslope that may have collected fines from the overlying Rose Hill Formation (Figure 6). An argillic layer is hypothesized to have formed on the more stable north-facing slope but not on the south-facing slope because of the long-term stability associated with aspect. This is further reflected in differences in particle size distribution between the two hillslopes, where more fine material is retained along the north-facing hillslope (Table 3, Figure 3).

4.1.4 | Accumulation of dust

Many lines of evidence, including bulk elemental composition, clay content, and $^{87}Sr/^{86}Sr$ ratios could also be consistent with atmospheric inputs of dust as a major source to the GR soils. To explore this idea, we estimated the time it would take for GR soil to be derived from dust, assuming the majority of the dust in this landscape was deposited during the LGM (Arvin et al., 2017) at rates of 30.8 ± 2.13 g m^{-2} year^{-1}, two orders of magnitude higher than today (0.29 ± 0.014 g m^{-2} year^{-1}). We also assumed that all of the soils in GR were derived from atmospheric deposition alone. Assuming a soil bulk density of 1.5 g cm^{-3}, it would have taken between 48 ka (LGM rates) and 5.2 Ma (present-day rates) to create 1 m of soil from dust alone. This mass balance calculation suggests that 1 m-thick GR soils could easily have developed entirely from dust within the 150 ka residence time for soils (Del Vecchio et al., 2018). Thus, the estimated deposition rates, mineral and element mass balances, and $^{87}Sr/^{86}Sr$ isotopic ratios of the soils all point to dust as another important source of nutrients (but not the sole contributor) to GR.

4.1.5 | Mixing model for soils in Garner Run

As discussed throughout, the four soil profiles studied in GR each show different extents of contribution from underlying Tuscarora bedrock, overlying Rose Hill residua, and dust (or Castanea) inputs. To estimate the relative contributions (and compare this to SH soils), we present a three-endmember mixing model [Equations 3 and 4)] (Marcon, 2019): f_i is the fraction of Tuscarora ($i = Tus$), Rose Hill ($i = RH$), and dust ($i = dust$) contributing to the soil:

$$f_{dust} + f_{RH} + f_{Tus} = 1 \quad (3)$$

The model was simultaneously constrained using $^{87}Sr/^{86}Sr$ ratios and six major elements (Al, Ca, Fe, K, Mg, Si) [Equation 4] to reconstruct the observed isotopic ratios and chemistry of the soil, $[X]_{soil}$ (Table 4). $[X]$ is the concentration of element X or value of $^{87}Sr/^{86}Sr$ ratio in each source:

$$[X]_{soil} = f_{dust}[X]_{dust} + f_{RH}[X]_{RH} + f_{Tus}[X]_{Tus} \quad (4)$$

For the north-facing GR soil (LRRT), we estimated that ~30% of the soil could be derived from Rose Hill Formation residua + dust/Castanea and the rest from Tuscarora (Table 1). In contrast, no dust or residua is required to explain SH soil (Jin et al., 2010; Marcon, 2019). As expected, endmember contributions also vary with aspect: more dust and residual shale is needed to account for the soil chemistry on the north-facing than the south-facing hillslopes (Table 1, Figure 6). Apparently, more extensive mass wasting and winnowing of fines from the south-facing dip-slope has created sandier soils with more Tuscarora contribution (i.e. more quartz content), while the north-facing slope has accumulated more dust/Castanea and residual Rose Hill materials. As discussed above, this is consistent with the patterns of mass wasting on the hillsides (Figure 7).

4.2 | Collector or producer landscapes for nutrients

Overall, the residence time of soils in SH (~20 ka) is much shorter than GR (~150 ka), and less colluvial materials mobilized during glacial periods have remained in the SH watershed compared to GR. In addition, ample evidence documents retention of dust in GR soils, whereas little to no evidence shows net element accumulation in the SH soils from the atmosphere (other than recent inputs of a few industrially derived trace metals such as Mn and Pb; Herndon et al., 2011). Fine particles are observed to be exported from soil and weathered rock in the SH stream and groundwater without subsurface retention (Kim et al., 2018). In contrast, fine particles—presumed to derive both from dust and from overlying shale—are retained in GR boulders underlying the hillslopes and valley (Figure 4).

Given these observations, we conclude that GR is a *collector* landscape [i.e. a landscape where both residual (material remaining in the watershed from strata that has long since weathered away, e.g. Rose Hill shale) and exogenous materials (e.g. dust) accumulate over soil production time scales (~150 ka) to influence soil chemistry]. We propose that these results likely explain the observations at the other four paired sandstone/shale sites as well. Attesting to this extrapolation, we note that metres-thick soils with long residence times are typical along sandstone ridgelines and thinner soils along shale ridgelines throughout the northern Appalachians (Ciolkosz et al., 1990). In *collector* landscapes, mass flux into the soil—including the chemical and physical disaggregation of bedrock into soil—is greater than the mass flux out when averaged over millennia (Figure 7). In GR, the Tuscarora Formation, a ridge-forming sandstone that weathers slowly and resists physical erosion (Ciolkosz et al., 1990), may be particularly effective as a *collector* landscape because of the synclinal nature of the structure (Figure 1). The slow erosion rates and trapping nature of the resistant sandstone in GR explain today's thick and relatively nutrient-rich soil. In contrast, we infer that SH acts as a landscape that erodes at rates that are roughly equivalent to the rates of soil production, resulting in relatively short soil residence times and less evidence for influence by exogenous materials into the soil. Given that the dominant source of nutrients to these shale soils is soil production from underlying bedrock, we refer to these as *producer* landscapes.

In comparison to shale systems (Tables 1 and 2), the higher concentrations of bioavailable P in soils, the higher concentrations of P in live leaves, and the lower percentage resorption of leaf P relative to N in sandstone systems is consistent with sandstone soils acting as collectors of P by accumulating dust and residua from overlying lithologies, while shale soils act as producers of P from the underlying bedrock.

4.3 | Vegetation

It has also been argued that ecosystems compensate for low nutrient content in soils by more efficiently recycling and retaining nutrients (Castle & Neff, 2008; Wardle et al., 2004). This points to another possibility for the differences between sandstone and shale soils (Table 1), namely that differences in vegetation or associated microbiota that develop on different geological substrates (e.g. Asner et al., 2014) affect P retention and throughput either directly or through complex feedbacks (e.g. Porder et al., 2015). Very small differences in P recycling in soils and vegetation over time could explain why P concentrations are similar to or greater in sandstone soils than in shale soils, even though initial P concentrations in bedrock are similar.

Although Equation 3 yields estimates of sources in very broad-brush fashion, we used it here to further calculate expected P concentrations for the soil using the known P concentrations in each source, and the calculated fraction of each source from the previously described three-endmember model (Marcon, 2019). The difference between this predicted P concentration and the measured concentration in the soil was attributed to P retained through soil–vegetation cycling. In GR, this predicted soil P concentration is about half the measured value, whereas in SH the calculated value is two-thirds the measured value. Although a more complete model is needed to constrain the system more precisely, it is possible that the larger discrepancy for sandstone could point to tighter recycling of P in the soil of that rock type compared to the shale. A number of mechanisms could explain such hypothetically tighter biotic P retention on the sandstone site, including differences in tree species, organic matter accumulation, Fe and Al oxyhydroxide accumulation, tree-associated

mycorrhizal fungal species, or bacteria-to-fungi ratios in soils (Brubaker et al., 2018; Walker & Syers, 1976; Wardle et al., 2004).

4.4 | Fate of fine particles in Garner Run

One puzzle about the quartz-rich sandy sediments observed in the GR valley (Figure 4) is that, although they are consistent with the underlying Tuscarora bedrock, they are not consistent with clay-containing soils along the hillslopes (Hoagland et al., 2017). Likewise, the colluvial and alluvial deposits in the SH valley floor are more sand-rich than the hillside soils. At SH, groundwater transport of fine particles out of the subsurface has been documented to have removed fines for geologically long time periods (Kim et al., 2018). We propose that the elevated turbidities and high iron contents of groundwaters in the valley in GR (borehole HV1) could similarly explain the contrast between clay-rich hillslope soils and sand-rich valley fill for GR. Specifically, ~80–97% of iron measured in waters sampled in the groundwater at GR was particulate rather than dissolved, and could therefore reflect transport of particles out of the GR valley in groundwater (Table S4). Loss of fine particles from GR hillslopes is likely accelerated by the stream's high connectivity to hillslopes because of the presence of large sandstone boulders and sandy soils (Xiao et al., 2019).

Evidence for subsurface transport of fine particles at GR is also provided by the microscopic imaging of Fe-oxide particles lodged within the pore throats of buried sandstone clasts sampled under hillslope soils and in valley fill (Figure 4). Such particles are unlikely to have precipitated from solutions carrying dissolved Fe (III) because the volume of advecting water required to carry sufficient dissolved Fe (III) through the fine pores and low overall porosity in the sandstone would be too large (Table 3). Such a conclusion is based on the generally low solubility of ferric-iron-containing minerals in neutral pH waters with low organic carbon. We infer that iron and clays are transported as fine particles in downward-infiltrating porewaters through the soils, into pores and through fractures within the weathering bedrock, and out of the catchments in both GR and SH; some of these particles remain lodged in sandstone pores in GR.

5 | CONCLUSIONS

Ecosystem maintenance and nutrient cycling within the CZ is known to be influenced by the concentration of lithogenic nutrients in the underlying substrate and the soil production rate. This study shows that the nature of a landscape as a *collector* is also important. Namely, we observed that slowly eroding sandstone watersheds in the northern Appalachians retain (and possibly recycle) more P over time as compared to faster-eroding shale watersheds. Soils developed on shale bedrock tend towards a balance between rock-derived P and losses of P to erosion. We emphasize that the variability in timing of ecosystem decline (Wardle et al., 2004) over long geological time periods is thus strongly influenced by the *collector* nature of a landscape and not just by the initial P concentration and the rate of erosion. *Collector* landscapes maintain peak productivity longer and delay ecosystem decline through the geological retention of limiting lithogenic nutrients such as P. In some cases, the collector nature of the landscape may also be characterized by tighter nutrient cycling within the soil. Our original intent was to explore the observation by Brubaker et al. (2018) and Reed and Kaye (2020) that biomass on shale is generally higher than on sandstone in our study area. We discovered that their observation is not well explained by differences in P concentrations and bedrock erosion rates between the two substrates, as we had hypothesized. Rather, the original explanation proposed by Reed and Kaye (2020) is strengthened (i.e. that differences in biomass are largely due to physical attributes related to the substrates, such as topography, clay content, and water-holding capacity). We add that the collector nature of the substrate is also an important attribute affecting ecosystem productivity.

ACKNOWLEDGEMENTS

This work was supported by the National Science Foundation for the Susquehanna Shale Hills Critical Zone Observatory to SLB (EAR 13–31726), the Department of Geosciences of The Pennsylvania State University, Hiroshi and Koya Ohmoto Fellowship 2017 for VM, and the Strategic Priority Research Programme of the Chinese Academy of Sciences (Grant No. XDB26000000), the National Science Foundation of China (Grant No. 41772380) and the Youth Innovation Promotion Association CAS fellowship (2019067) to WL. Shale Hills research was conducted in Penn State's Stone Valley Forest, which is funded by the Penn State College of Agriculture Sciences, Department of Ecosystem Science and Management and managed by the staff of the Forestlands Management Office. Garner Run research was conducted in Rothrock State Forest, which is funded and managed by the Pennsylvania Department of Conservation and Natural Resources, Bureau of Forestry. We thank L. Hill for the data for bioavailable and foliar nutrients and W. Reed, K. Brubaker, B. Forsythe, D. Eissenstat, M. Kaye, and J. Del Vecchio for input and field expertise. VM did field, laboratory, and computational work; SLB supervised the project; BH, XG, WL, JK, and RD contributed data, interpretations, and writing.

CONFLICT OF INTEREST

The authors have no conflict of interest to declare with respect to this work.

DATA AVAILABILITY STATEMENT

The data that support the findings of this study are available in the main body of the paper, or in the supplementary material to this paper, or in cited works that are available to the public.

ORCID

Virginia Marcon https://orcid.org/0000-0003-4423-0601
Beth Hoagland https://orcid.org/0000-0001-7275-6091
Roman A. DiBiase https://orcid.org/0000-0002-5347-8396
Susan L. Brantley https://orcid.org/0000-0002-9574-2693

REFERENCES

Aarons, S.M., Blakowski, M.A., Aciego, S.M., Stevenson, E.I., Sims, K.W.W., Scott, S.R. & Aarons, C. (2017) Geochemical characterization of critical dust source regions in the American West. *Geochimica et Cosmochimica Acta*, 215, 141–161. https://doi.org/10.1016/j.gca.2017.07.024

Aciego, S.M., Riebe, C.S., Hart, S.C., Blakowski, M.A., Carey, C.J., Aarons, S. M., *et al*. (2017) Dust outpaces bedrock in nutrient supply to montane forest ecosystems. *Nature Communications*, 8(1), 14800. https://doi.org/10.1038/ncomms14800

Alexander, E.B. (1985) Rates of soil formation from bedrock or consolidated sediments. *Physical Geography*, 6(1), 25–42. https://doi.org/10.1080/02723646.1985.10642261

Anderson, S.P., Dietrich, W.E. & Brimhall, G.H. (2002) Weathering profiles, mass-balance analysis, and rates of solute loss: linkages between weathering and erosion in a small, steep catchment. *Geologic Society of American Bulletin*, 114, 1143–1158.

Arvin, L.J., Riebe, C.S., Aciego, S.M. & Blakowski, M.A. (2017) Global patterns of dust and bedrock nutrient supply to montane ecosystems. *Science Advances*, 3(12), eaao1588. https://doi.org/10.1126/sciadv.aao1588

Asner, G.P., Martin, R.E., Tupayachi, R., Anderson, C.B., Sinca, F., Carranza-Jimenez, L. & Martinez, P. (2014) Amazonian functional diversity from forest canopy chemical assembly. *Proceedings of the National Academy of Sciences of the United States of America*, 111(15), 5604–5609. https://doi.org/10.1073/pnas.1401181111

Bern, C.R. & Yesavage, T. (2018) Dual-phase mass balance modeling of small mineral particle losses from sedimentary rock-derived soils. *Chemical Geology*, 476, 441–455.

Boerner, R.E. (1984) Foliar nutrient dynamics and nutrient use efficiency of four deciduous tree species in relation to site fertility. *Journal of Applied Ecology*, 21(3), 1029–1040. https://doi.org/10.2307/2405065

Brantley, S.L., DiBiase, R.A., Russo, T.A., Shi, Y., Lin, H., Davis, K.J., *et al*. (2016) Designing a suite of measurements to understand the critical zone. *Earth Surface Dynamics*, 4, 211–235. https://doi.org/10.5194/esurf-5194-5211-2016

Brantley, S.L., Holleran, M., Jin, L. & Bazilevskaya, E. (2013) Probing deep weathering in the Shale Hills Critical Zone Observatory, Pennsylvania (USA): the hypothesis of nested chemical reaction fronts in the subsurface. *Earth Surface Processes and Landforms*, 38(11), 1280–1298. https://doi.org/10.1002/esp.3415

Brantley, S.L., White, T.S., West, N., Williams, J., Forsythe, B., Shapich, D., *et al*. (2018) Susquehanna Shale Hills Critical Zone Observatory: shale hills in the context of Shaver's Creek watershed. *Vadose Zone Journal*, 17, 180092. https://doi.org/10.2136/vzj182018.180004.180092

Brimhall, G.H. & Dietrich, W.E. (1987) Constitutive mass balance relations between chemical composition, volume, density, porosity, and strain in metasomatic hydrochemkai systems: results on weathering and pedogenesis. *Geochimica et Cosmochimica Acta*, 51, 567–587.

Brubaker, K.M., Johnson, Q.K. & Kaye, M.W. (2018) Spatial patterns of tree and shrub biomass in a deciduous forest using leaf-off and leaf-on lidar. *Canadian Journal of Forest Research*, 48(9), 1020–1033. https://doi.org/10.1139/cjfr-2018-0033

Brush, G., Lenk, C. & Smith, J. (1980) The natural forests of Maryland: an explanation of the begetation map of Maryland. *Ecological Monographs*, 50, 77–92.

Capo, R.C., Stewart, B.W. & Chadwick, O.A. (1998) Strontium isotopes as tracers of ecosystem processes: theory and methods. *Geoderma*, 82(1–3), 197–225. https://doi.org/10.1016/S0016-7061(97)00102-X

Castle, S.C. & Neff, J.C. (2008) Plant response to nutrient availability across variable bedrock geologies. *Ecosystems*, 12, 101–113.

Chadwick, O.A., Derry, L.A., Vitousek, P.M., Huebert, B.J. & Hedin, L.O. (1999) Changing sources of nutrients during four million years of ecosystem development. *Nature*, 397(6719), 491–497. https://doi.org/10.1038/17276

Ciolkosz, E.J., Carter, B.J., Hoover, M.T., Cronce, R.C., Waltman, W.J. & Dobos, R.R. (1990) Genesis of soils and landscapes in the Ridge and Valley province of central Pennsylvania. *Geomorphology*, 3(3–4), 245–261. https://doi.org/10.1016/0169-555X(90)90006-C

Cotter, E. (1983) Shelf, paralic, and fluvial environments and eustatic sea-level fluctuations in the origin of the Tuscarora Formation (Lower Silurian) of central Pennsylvania. *Journal of Sedimentary Petrology*, 53, 25–49.

Crock, J.G., Lichte, F.E. & Briggs, P.H. (1983) Determination of elements in National Bureau of Standards' Geological Reference Materials SRM 278 Obsidian and SRM 688 Basalt by Inductively Coupled Argon Plasma-Atomic Emission Spectrometry. *Geostandards Newsletter*, 7(2), 335–340. https://doi.org/10.1111/j.1751-908X.1983.tb00395.x

Del Vecchio, J., DiBiase, R.A., Denn, A.R., Bierman, P.R., Caffee, M.W. & Zimmerman, S.R.H. (2018) Record of coupled hillslope and channel response to Pleistocene erosion and deposition in a sanstone headwater valley, central Pennsylvania. *Geological Society of America Bulletin*, 130, 1903–1917. https://doi.org/10.1130/B31912.31911

Derry, L.A. & Chadwick, O.A. (2007) Contributions from Earth's atmosphere to soil. *Elements*, 3, 333–338.

Elliott, P.E. & Drohan, P.J. (2009) Clay accumulation and argillic-horizon development as influenced by aeolian deposition vs. local parent material on quartzite and limestone-derived alluvial fans. *Geoderma*, 151(3–4), 98–108. https://doi.org/10.1016/j.geoderma.2009.03.017

Farmer, A.M. (1993) The effects of dust on vegetation: a review. *Environmental Pollution*, 79(1), 63–75. https://doi.org/10.1016/0269-7491(93)90179-R

Folk, R.L. (1960) Petrography and origin of the Tuscarora, Rose Hill, and Keefer Formations, lower and middle Silurian of eastern West Virginia. *Journal of Sedimentary Petrology*, 30, 1–58.

Gardner, T.W., Ritter, J.B., Shuman, C.A., Bell, J.C., Sasowsky, K.C. & Pinter, N. (1991) A periglacial stratified slope deposit in the Valley and Ridge Province of central Pennsylvania, USA: sedimentology, stratigraphy, and geomorphic evolution. *Permafrost and Periglacial Processes*, 2(2), 141–162. https://doi.org/10.1002/ppp.3430020208

Grousset, F.E. & Biscaye, P.E. (2005) Tracing dust sources and transport patterns using Sr, Nd and Pb isotopes. *Chemical Geology*, 222, 149–167.

Hahm, W.J., Riebe, C.S., Lukens, C.E. & Araki, S. (2014) Bedrock composition regulates mountain ecosystems and landscape evolution. *Proceedings of the National Academy of Sciences*, 111, 3338–3343.

Herndon, E.M., Jin, L. & Brantley, S.L. (2011) Soils reveal widespread manganese enrichment from industrial inputs. *Environmental Science & Technology*, 45(1), 241–247. https://doi.org/10.1021/es102001w

Hill L. 2017. *Lithologic controls on soil properties of temperate forest ecosystems in central Pennsylvania*. MS thesis, Pennsylvania State University, USA.

Hoagland, B., Russo, T.A., Gu, X., Hill, L., Kaye, J., Forsythe, B. & Brantley, S.L. (2017) Hyporheic zone influences on concentration–discharge relationships in a headwater sandstone stream. *Water Resources Research*, 53(6), 4643–4667. https://doi.org/10.1002/2016WR019717

Jin, L., Ravella, R., Ketchum, B., Bierman, P.R., Heaney, P., White, T. S. & Brantley, S.L. (2010) Mineral weathering and elemental transport during hillslope evolution at the Susquehanna/Shale Hills Critical Zone Observatory. *Geochimica et Cosmochimica Acta*, 74, 3669–3691.

Keestra, S.D., Bouma, J., Wallinga, J., Tittonell, P., Smith, P., Cerdà, A., *et al*. (2016) The significance of soils and soil science towards realization of the United Nations Sustainable Development Goals. *The Soil*, 2(2), 111–128. https://doi.org/10.5194/soil-2-111-2016

Kennedy, M.J., Chadwick, O.A., Vitousek, P.M., Derry, L.A. & Hendricks, D. M. (1998) Changing sources of base cations during ecosystem development, Hawaiian Islands. *Geology*, 26(11), 1015–1018. https://doi.org/10.1130/0091-7613(1998)026<1015:CSOBCD>2.3.CO;2

Kim, H., Gu, X. & Brantley, S.L. (2018) Particle fluxes in groundwater change subsurface shale rock chemistry over geologic time. *Earth and Planetary Science Letters*, 500, 180–191. https://doi.org/10.1016/j.epsl2018.1007.1031

Lawrence, C.R. & Neff, J.C. (2009) The contemporary physical and chemical flux of aeolian dust: a synthesis of direct measurements of dust deposition. *Chemical Geology*, 267(1–2), 46–63. https://doi.org/10.1016/j.chemgeo.2009.02.005

Li, L., DiBiase, R.A., Del Vecchio, J., Marcon, V., Hoagland, B., Xiao, D., *et al*. (2018) The effect of lithology and agriculture at the Susquehanna Shale Hills Critical Zone Observatory (SSHCZO). *Vadose Zone*

Journal, 17, 180063. https://doi.org/10.2136/vzj182018.180003.180063

Ma, L., Chabaux, F., Pelt, E., Blaes, E., Jin, L. & Brantley, S. (2010) Regolith production rates calculated with uranium-series isotopes at Susquehanna/Shale Hills Critical Zone Observatory. *Earth and Planetary Science Letters*, 297(1–2), 211–225. https://doi.org/10.1016/j.epsl.2010.06.022

Ma, L., Chabaux, F., West, N., Kirby, E., Jin, L. & Brantley, S. (2013) Regolith production and transport in the Susquehanna Shale Hills Critical Zone Observatory, part 1: insights from U-series isotopes. *Journal of Geophysical Research – Earth Surface*, 118(2), 722–740. https://doi.org/10.1002/jgrf.20037

Marcon V. 2019. *The effect of lithology on (bio)geochemical weathering: sandstone to serpentinite*. PhD thesis, Pennsylvania State University, USA.

Meek, K., Derry, L., Sparks, J. & Cathles, L. (2016) $^{87}Sr/^{86}Sr$, Ca/Sr, and Ge/Si ratios as tracers of solute sources and biogeochemical cycling at a temperate forested shale catchment, central Pennsylvania, USA. *Chemical Geology*, 445, 84–102.

Miller, S.R., Sak, P.B., Kirby, E. & Bierman, P.R. (2013) Neogene rejuvenation of central Appalachian topography: evidence for differential rock uplift from stream profiles and erosion rates. *Earth and Planetary Science Letters*, 369, 1–12.

National Research Council. (2001) *Basic Research Opportunities in Earth Science*. Washington, D.C.: National Academy Press.

Porder, S. & Hilley, G.E. (2011) Linking chronosequences with the rest of the world: predicting soil phosphorus content in denuding landscapes. *Biogeochemistry*, 102, 153–166.

Porder, S., Johnson, A.H., Xing, H.X., Brocard, G., Goldsmith, S. & Pett-Ridge, J. (2015) Linking geomorphology, weathering and cation availability in the Luquillo Mountains of Puerto Rico. *Geoderma*, 249, 100–110.

Porder, S. & Ramachandran, S. (2013) The phosphorus concentration of common rocks – a potential driver of ecosystem P status. *Plant and Soil*, 367(1–2), 41–55. https://doi.org/10.1007/s11104-012-1490-2

Porder, S., Vitousek, P.M., Chadwick, O.A., Chamberlain, C.P. & Hilley, G.E. (2007) Uplift, erosion, and phosphorus limitation in terrestrial ecosystems. *Ecosystems*, 10, 158–170.

Portenga, E.W., Bierman, P.R., Rizzo, D.M. & Rood, D.H. (2013) Low rates of bedrock outcrop erosion in the central Appalachian Mountains inferred from in situ Be-10. *Geological Society of America Bulletin*, 125(1–2), 201–215. https://doi.org/10.1130/B30559.1

Reed, W.P. & Kaye, M.W. (2020) Bedrock type drives forest carbon storage and uptake across the mid-Atlantic Appalachian Ridge and Valley, USA. *Forest Ecology and Management*, 460, 117881. https://doi.org/10.1016/j.foreco.2020.117881

Romaniello, S.J., Field, M.P., Smith, H.B., Gordon, G.W., Kim, M.H. & Anbar, A.D. (2015) Fully automated chromatographic purification of Sr and Ca for isotopic analysis. *Journal of Analytical Atomic Spectrometry*, 30(9), 1906–1912. https://doi.org/10.1039/C5JA00205B

Schultz L. 1964. *Quantitative interpretation of mineralogical composition from x-ray and chemical data for the Pierre shale* U.S. Geological Survey Professional Paper 391-C.

Sevon WD. 1984. *A sandstone weathering rate from northeastern Pennsylvania*. Geological Society of America Abstracts with Programs No. 63.

Smith, L.A., Eissenstat, D.M. & Kaye, M.W. (2017) Variability in aboveground carbon driven by slope aspect and curvature in an eastern deciduous forest, USA. *Canadian Journal of Forest Research*, 47, 149–158. https://doi.org/10.1139/cjfr-2016-0147

Sullivan, P.L., Hynek, S.A., Gu, X., Singha, K., White, T., West, N., *et al.* (2016) Oxidative dissolution under the channel leads geomorphological evolution at the Shale Hills catchment. *American Journal of Science*, 316, 981–1026. https://doi.org/10.2475/1010.2016.1002

Tye, A.M., Lawley, R.L., Ellis, M.A. & Rawlins, B.G. (2011) The spatial variation of weathering and soil depth across a Triassic sandstone outcrop. *Earth Surface Processes and Landforms*, 36, 569–581.

Walker, T.W. & Syers, J.K. (1976) The fate of phosphorous during pedogenesis. *Geoderma*, 15, 1–19.

Wardle, D.A., Walker, L.R. & Bardgett, R.D. (2004) Ecosystem properties and forest decline in contrasting long-term chronosequences. *Science*, 305(5683), 509–513. https://doi.org/10.1126/science.1098778

West, N., Kirby, E., Bierman, P.R. & Clarke, B.A. (2014) Aspect-dependent variations in regolith creep revealed by meteoric ^{10}Be. *Geology*, 42(6), 507–510. https://doi.org/10.1130/G35357.35351

West, N., Kirby, E., Nyblade, A. & Brantley, S. (2019) Climate preconditions the critical zone: elucidating the role of subsurface fractures in the evolution of asymmetric topography. *Earth and Planetary Science Letters*, 513, 197–205. https://doi.org/10.1016/j.epsl.2019.1001.1039

Wolf, A.M. & Beegle, D.M. (2011) Recommended soil pH and lime requirement tests. In: Sims, T.J. & Wolf, A. (Eds.) *Recommended Soil Testing Procedures for the Northeastern United States*, 3rd edition. Newark, DE: University of Delaware, pp. 11–16.

Xiao, D., Shi, Y., Brantley, S.L., Forsythe, B., DiBiase, R., Davis, K. & Li, L. (2019) Streamflow generation from catchments of contrasting lithologies: the role of soil properties, topography, and catchment size. *Water Resources Research*, 55, 9234–9257. https://doi.org/10.1029/2018WR023736

Yesavage, T.A., Fantle, M.S., Vervoort, J., Mathur, R., Jin, L., Liermann, L.J. & Brantley, S.L. (2012) Fe cycling in the Shale Hills Critical Zone Observatory, Pennsylvania: an analysis of biogeochemical weathering and Fe isotope fractionation. *Geochimica et Cosmochimica Acta*, 99, 18–38. https://doi.org/10.1016/j.gca.2012.1009.1029

Yu, H., Chin, M., Yuan, T., Bian, H., Remer, L.A., Prospero, J.M., *et al.* (2015) The fertilizing role of African dust in the Amazon rainforest: a first multiyear assessment based on data from Cloud-Aerosol Lidar and Infrared Pathfinder Satellite Observations. *Geophysical Research Letters*, 42(6), 1984–1991. https://doi.org/10.1002/2015GL063040

SUPPORTING INFORMATION

Additional supporting information may be found in the online version of the article at the publisher's website.

How to cite this article: Marcon, V., Hoagland, B., Gu, X., Liu, W., Kaye, J., DiBiase, R.A. et al. (2021) How the capacity of bedrock to collect dust and produce soil affects phosphorus bioavailability in the northern Appalachian Mountains of Pennsylvania. *Earth Surface Processes and Landforms*, 46(14), 2807–2823. Available from: https://doi.org/10.1002/esp.5209